



LiNbCoX (X = Al, Ga) quaternary Heusler compounds for high-temperature thermoelectric properties: a computational approach

JASPAL SINGH¹, TAVNEET KAUR^{2,*} , AMRIT PAL SINGH^{3,4}, MEGHA GOYAL², KULWINDER KAUR⁵, SHAKEEL AHMAD KHANDY⁶, ISHTIHADAH ISLAM⁷, AADIL FAYAZ WANI⁸, RAM KRISHAN⁹, M M SINHA² and S S VERMA²

¹Department of Physics, Mata Sundri University Girls College, Mansa, PB 151505, India

²Department of Physics, Sant Longowal Institute of Engineering and Technology (Deemed University), Sangrur, PB 148106, India

³Health Physics Unit, Nuclear Fuel Complex, Hyderabad 500062, India

⁴Homi Bhabha National Institute, Mumbai 400094, India

⁵Department of Physics, Mehar Chand Mahajan DAV College for Women, Chandigarh 160036, India

⁶Zhejiang University, Hangzhou 310027, China

⁷Department of Physics, Jamia Millia Islamia, New Delhi 110025, India

⁸Department of Applied Sciences, Punjab Engineering College (Deemed to be University), Chandigarh 160012, India

⁹Department of Computer Science, Mata Sundri University Girls College, Mansa, PB 151505, India

*Author for correspondence (tavneetkaur001@gmail.com)

MS received 14 November 2022; accepted 2 February 2023

Abstract. Researchers have looked into quaternary Heusler (QH) compounds for their potential use in futuristic gadgets like photovoltaic cells, optical fibres, thermoelectric modules and spintronic sensors. As per such motivations and research interests, here we are presenting two recently reported Li-based QH compounds LiNbCoAl and LiNbCoGa which are stabilized into face-centred cubic structure of space group F-43m with semiconducting nature. These compounds exhibit high melting temperatures, showing the p-type semiconducting nature and are found to have advantageous thermoelectric capabilities in the high-temperature range. Additionally, the dynamical stability and appropriate elastic and mechanical characteristics for the foundation of effective thermoelectric modules in the temperature range of 1600 K enhance their scientific and technical scope. The electronic band structure is discussed along with the density of states for the better understanding of the electrical properties. The thermodynamic response up to a temperature of 1600 K is also examined for understanding in terms of free energy, specific heat at constant volume and entropy. The special dependences in the two and three dimensions are applied and investigated to characterize the anisotropic nature. However all the required thermoelectric properties are calculated and presented, and the highest figure of merit value at 1600 K for both materials is 0.47 for LiNbCoAl and 0.56 for LiNbCoGa, respectively. As per their excellent practical properties, the current study asserts that both QH compounds should really be considered for energy conversion techniques in high-temperature environments. For the complete study prospectus, these materials are being disclosed for the first time here.

Keywords. Lattice thermal conductivity; phonons; thermoelectric characteristics; density functional theory; the figure of merit.

1. Introduction

The focus of current research is on ways for creating pollution-free energy that can considerably aid in solving the world's energy crisis. Thermoelectricity is a viable option for turning excess heat into usable electricity [1–5]. Since the functioning of thermoelectric modules (related to thermoelectric materials) produces no pollution, thermoelectricity has been named 'A Green Technology' for the future [6]. It is possible to evaluate the thermoelectric efficiency of

a material using the relation utilizing a dimensionless measure known as the Figure of Merit (ZT) for measuring the thermoelectric efficiency of material:

$$ZT = \frac{S^2 \sigma}{k_e + k_l} T \quad (1)$$

Here the symbols have their conventional meanings. However the symbols k_e and k_l refer to the electronic and lattice portions of the thermal conductivity in this context, respectively, and their sum ($k_t = k_e + k_l$) denotes the

material's overall total thermal conductivity [7]. Even though many scientists are currently looking for materials with high figures of merit, only a small fraction of materials at normal temperatures reached the unit value ($ZT = 1$) [8–10]. Modern research is facing challenges to find and develop a class of materials that is enriched by mechanical and electrical aspects and can be utilized as thermoelectric elements. In such times a new class of materials, i.e., Heusler compounds can fulfil all such requirements. Friedrich Heusler (1903) first proposed this class of Heusler compounds, which stabilizes in the face-centred cubic (FCC) structure as group F-43m with intermetallic semi-conducting nature. These materials exist as full-Heusler and half-Heuslers (HH), which have improved mechanical properties and are finding new uses in photovoltaic, optical and thermoelectric devices [11–13]. However using an appropriate electropositive element, such as Li, in compliance with the 18-valence electron count (VEC) rule, any eligible spaces between HH or full-Heuslers (FH) are filled to form a new compound, which is recommended as the Quaternary Heusler (QH) compound. Some HH and full-Heuslers have been singled out as particularly interesting materials for topological devices, spintronics and ferromagnetism in the rapidly growing subject of superconductivity [14–17]. Slack and Rowe [18] also noted that effective thermoelectric materials have low bandgaps of semiconducting nature and phonon-glass electron crystal behaviour [18]; these suitable characteristics are found in the Heusler family. Heusler materials have attracted study attention due to their non-toxic nature, superior thermodynamic and mechanical characteristics, semiconducting behaviour and affordable availability [19–23]. Some of the earth's crust elements with the lowest prices have shown exceptional thermoelectric capabilities [24], in contrast to the usually efficient thermoelectric materials. There are just a few Heusler systems, for which recent research shows that their thermoelectric properties are far superior to those of more popular thermoelectric materials across a large temperature range [25,26]. Thermoelectric properties comparable with modern applications are found in the two widely studied Ti, Hf and Zr based HH materials [27,28] that are being considered in the various research visions due to their multifunctional properties. Thermoelectricians are quite interested when recently some n-type and p-type HH with ZT values of around 0.8 and 1.05 at extreme temperatures [29] are explored with many of the supporting qualities. One of the Sb-based HH has been recommended with $ZT > 1$ with futuristic trends [30,31], which is also a recommending feature to investigate this class of materials. According to Heusler's alloy $Nb_{0.6}Ta_{0.4}Ti_{0.2}FeSb$ [32], the peak ZT is 1.6 at 1200 K, which bodes well for the future of the thermoelectric sector. HH $LaPtSb$ [33] is a marvel in the field of energy conversion research with a ZT of 2.2 at room temperature. He *et al* [34] explored some Heuslers in recent years using both practical and theoretical study methods from density functional theory (DFT) that all are acquiring

improved mechanical characteristics. They also found that all of the compounds exhibit exceptional thermoelectric capabilities and incredibly low lattice thermal conductivity. First-principles calculations were used by Haleoot and Hamad (2020) to achieve such goals; they analysed some QH with multifunctioning approaches [35]. A new QH compound $CrVNbZn$ [36] using DFT also has been studied to achieve results. It exhibits excellent electronic and magnetic properties as well as a peak value of $ZT = 0.79$ over a wide temperature range of 260 to 480 K. Similarly $LiScPdPb$, $LiTiCoSi$ and $LiTiCoGe$ are three examples of Li-based QH compounds that have already undergone extensive study [37,38] that are notable for their thermoelectric properties in addition to their structural, electronic and phonon characteristics. He *et al* [39] recently found two new Li-based QH compounds ($LiNbCoAl$ and $LiNbCoGa$) and were analysed utilizing theoretical research techniques, i.e., DFT and Boltzmann transport equations. These two Li-based QH compounds were reported to have bandgaps of 0.465 and 0.810 eV, respectively. In the generalized gradient approximation, their bandgaps were determined using Perdew Burke Ernzerhof (PBE) potentials, and semiconducting behaviour was proclaimed using FCC structure of the F-43m space group. Due to their high melting temperatures (1996 K for $LiNbCoAl$) and (1912 K for $LiNbCoGa$) along with the conformity of the 18 Valence Electron Count norm, the two provided QHs have the potential to usher in a new era of effective thermoelectric materials in the high-temperature range. The dynamic stability of the compounds presented is assessed using calculations of the phonon dispersion curves and phonon density of states (PDOS) at the k-points of the first Brillouin zone. All additional mechanical and elastic parameters, including the bulk modulus and Debye's temperature, have been determined. The high melting point materials are examined in this study together with their Seebeck coefficient, electrical conductivity, electronic thermal conductivity, lattice thermal conductivity and figure of merit as functions of chemical potential over the wide temperature range of 1600 K. To evaluate the thermodynamic behaviour of both materials at 1600 K, all the specified thermodynamic parameters, including specific heat at constant volume, free energy and entropy, are calculate and presented.

2. Computational approach

The materials $LiNbCoAl$ and $LiNbCoGa$ are the focus of computational studies. The Boltzmann transport equations are used to conduct the computational study on $LiNbCoAl$ and $LiNbCoGa$ materials, along with the DFT, which is the recommended research tool of theoretical research. In the present study, Quantum ESPRESSO (QE) method has been employed using generalized gradient approximation [40–43] within Perdew Burke Ernzerhof (PBE) exchange-correlation functional in the plane wave pseudo-potential

approach. The structural optimization was carried out by using the plane wave basis set for both LiNbCoAl and LiNbCoGa, which is effective with 70 Ry cut-off energy. The $10 \times 10 \times 10$ k-mesh grid from the Monkhorst-Pack [44,45] is used for the Brillouin zone integration. Using a finer $20 \times 20 \times 20$ k-mesh, we determine the densities of states for both compounds. Elastic and mechanical properties may be extracted owing to the thermal pw.x package [46,47] included on QE drives. The variation of mechanical parameters have been calculated by ELATE online tool [48]. Utilizing the linear response density functional perturbation theory (DFPT) [49], the vibrational properties of primitive unit cell was determined. The Boltzmann transport equation is utilized to determine the thermoelectric properties, which is subsequently completed using the BoltzTraP algorithm [50–52]. In this instance, we employ two approximations: the rigid band approximation (RBA) and the constant relaxation time approximation. The following equations are used to calculate the transport properties:

$$\sigma_{\alpha\beta}(T; \mu) = \frac{1}{\Omega} \int \sigma_{\alpha\beta}(\varepsilon) \left[\frac{-\partial f_{\mu}(T; \varepsilon)}{\partial \varepsilon} \right] d\varepsilon \quad (2)$$

$$k_{\alpha\beta}^0(T; \mu) = \frac{1}{e^2 T \Omega} \int \sigma_{\alpha\beta}(\varepsilon) (\varepsilon - \mu)^2 \left[\frac{-\partial f_{\mu}(T; \varepsilon)}{\partial \varepsilon} \right] d\varepsilon \quad (3)$$

here, k^0 is the thermal conductivity of electrons, and the Seebeck coefficient may be found using the formula below:

$$S_{ij} = E_i (\nabla_j T)^{-1} = (\sigma^{-1}) \alpha_i v_{\alpha j} \quad (4)$$

where $v_{\alpha j}$ stands for band velocity, μ for chemical potential, ε for band energy and f_{μ} for band energy.

To simplify the calculations of thermoelectric properties, the default value of the relaxation time (τ) is taken as 10^{-14} s [53,54] and the melting point is determined by the below given relation [55,56]:

$$T_{\text{melt}} = [553K + \left(\frac{5.91K}{\text{GPa}} \right) C_{11}] \pm 300 K \quad (5)$$

The article begins with a discussion of the vibrational properties, then moves on to the elastic and mechanical properties, and finally concludes with the thermodynamic and thermoelectric properties, all of which serve to highlight the tremendous significance of the work presented here.

3. Results and discussion

3.1 Vibrational properties

The phonon dispersion curves-based vibrational properties of both QHs are shown in figure 1 along the high symmetry directions of the Brillouin zone, by estimating positive frequencies, dynamic stability is established for both QH alloys. Since there are three degrees of freedom for every

single one of the atoms that make up a typical unit cell, each compound's dispersion curve contains 12 vibrational modes that are related to the 4 atoms. The phonon dispersion curves show two distinct regions, the low-frequency zone (LFZ) and the high-frequency zone (HFZ). When comparing the same sequence of compounds, the LFZ range for LiNbCoAl and LiNbCoGa is 0 to 326.86 cm^{-1} and 0 to 236.41 cm^{-1} , respectively, while the HFZ range is 460.69 to 483.7 cm^{-1} and 449.49 to 461.51 cm^{-1} . The value of phonon modes diminishes on moving down the group from Al to Ga, owing to shorter bond length. For LiNbCoAl and LiNbCoGa, respectively, the spacing between the LFZ and HFZ is predicted to be 156.84 and 225.1 cm^{-1} . The difference in mass between the Li atom and the other atoms in the materials, which results from the fact that heavier atoms vibrate at a lower frequency than lighter atoms, causes a considerable gap to form between the two zones [57]. This fact can also be confirmed by the phonon density of states (PDOS) that are plotted along with the phonon curves. While the following nine phonon modes, starting at a greater value of zone center, are optical modes, the first three phonon modes presented, starting at zero value of zone center, are acoustic modes. Phonon dispersion curves (PDC) show a separation between longitudinal optical modes (LO) and transverse optical modes (TO), although these modes tend to degenerate beyond the point Γ of the Brillouin zone. From the PDOS curves, it is too clear that the lower mass atom Li contributes to higher phonon modes, while the higher mass atom Nb accounts for the acoustic modes in both the studied materials. The intermediate mass atoms of Co, Al/Ga in LiNbCoAl and LiNbCoGa play a part in the lower optical phonon modes.

3.2 Mechanical and elastic properties

To examine the existing compounds' mechanical robustness and elastic responsiveness, the elastic constants are calculated (C_{11} , C_{21} and C_{44}) and displayed in table 1. The term C_{44} depicts to overcome shearing distortions, whereas the elastic constant C_{11} gauges the stiffness of the material against primary stresses. Due to its fragility, a material with a high Frantsevich's ratio G/B is not a good element for thermoelectric applications. In this case, the ratios (G/B) for the compounds LiNbCoAl and LiNbCoGa are 0.59 and 0.60, respectively; demonstrating the brittle nature of both the compounds [58]. The following are the recommended stability criteria [59] that may be implemented to assess durability in mechanical use:

$$C_{11} - C_{12} > 0, C_{11} > 0, C_{44} > 0, \\ (C_{11} + 2C_{12}) > 0 \text{ and } C_{12} < B < C_{11} \quad (6)$$

The elasticity parameters mentioned above for both of the materials are listed in table 1 along with comparisons to other QH compounds [15]. Both materials have been proven to meet the mechanical requirements for improved

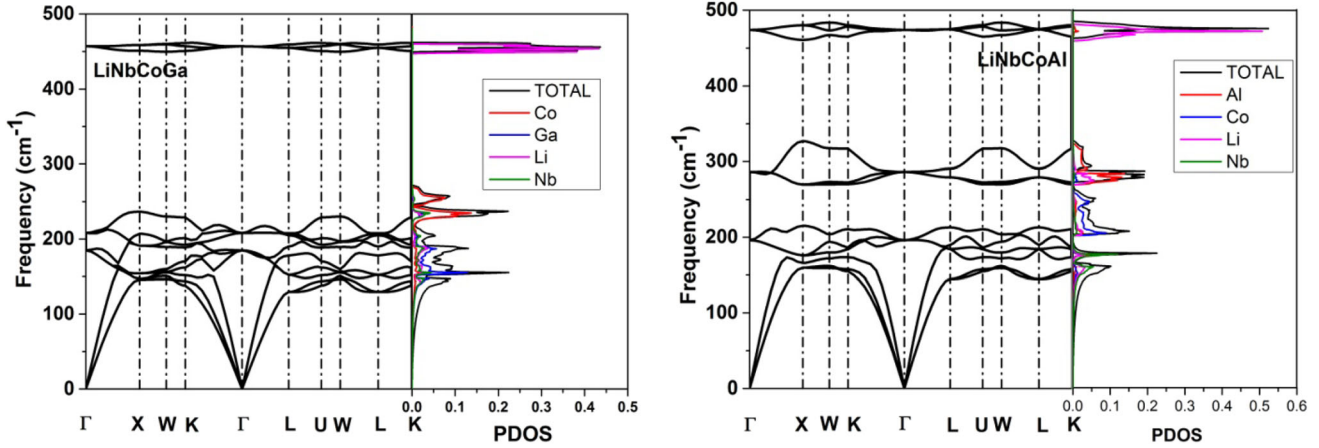


Figure 1. Density of states and phonon curves for both the presented QHs.

Table 1. QH compounds' estimated elastic constants.

Compounds	C_{11}	C_{12}	C_{44}	Ref.
LiNbCoAl	241	110	117	This study
LiNbCoGa	227	109	117	
CoZrMnAl	261.1481	115.4068	85.8098	[15]
CoZrMnGa	214.9019	108.7590	82.9659	[15]
CoZrMnGe	238.3834	65.3708	91.3630	[15]
CoZrMnIn	209.6486	117.0364	86.1891	[15]

thermoelectric module production. Additionally, the specified materials' bulk (B) and shear (G) moduli can be calculated using the Voigt-Reuss-Hill approximations (VRH) [60,61]. The hardness can be calculated using the equation:

$$H_V = 2 \left[\left(\frac{G}{B} \right)^2 G \right]^{0.585} - 3 \quad (7)$$

Similarly, table 2 displays a measure of hardness known as the Victor hardness factor (H_V) [62], this suggests that both the presenting semiconductors are more resilient than CoZrMnAl and CoZrMnGa. Both of the materials shown here have a higher Young's modulus (Y), a measure of stiffness, than the previously reported QH compounds CoZrMnAl, CoZrMnGa and CoZrMnGe. Shear anisotropy

factor (A) is determined for both compounds presented using the same relation.

$$A = \frac{2C_{44}}{C_{11} - C_{12}} \quad (8)$$

Since the computed values of A are bigger than 1, it may be concluded that these compounds are naturally anisotropic [38].

Furthermore, figures 2 and 3 illustrate the dimensional dependence of mechanical properties for LiNbCoAl and LiNbCoGa in three dimensions and along the xy , xz , and yz axes, including Young's modulus, linear compressibility, Shear modulus and Poisson ratio. The ELATE online software [48] is used for the research of elastic tensors. The three-dimensional mechanical parameter shapes in figures 2 and 3 are coloured green for the lowest values of the researched mechanical parameters and blue for the greatest values. Table 3 provides an overview of the maximum and minimum values of the aforementioned characteristics for both of the materials under investigation. The isotropic character of the material is demonstrated by the spherical shape of the directional dependency of mechanical properties. Only linear compressibility shows spherical symmetry, while all other properties have deviated from spherical symmetry for both of the compounds LiNbCoAl and LiNbCoGa. As a result, linear compressibility is determined to be an isotropic

Table 2. QH compound's estimated mechanical parameters.

Parameters	B , GPa	G , GPa	Y , GPa	A	ν	G/B	H_V	ζ	Ref.
LiNbCoAl	154	92	232	1.78	0.248	0.59	12.19	0.76	This study
LiNbCoGa	148	89	222	1.9	0.249	0.6	12.2	0.8	
CoZrMnAl	163.985	80.375	207.262	1.178	0.289	—	8.303	—	[15]
CoZrMnGa	144.139	69.358	179.312	1.563	0.292	—	7.148	—	[15]
CoZrMnGe	123.041	89.387	215.882	1.056	0.207	—	16.062	—	[15]

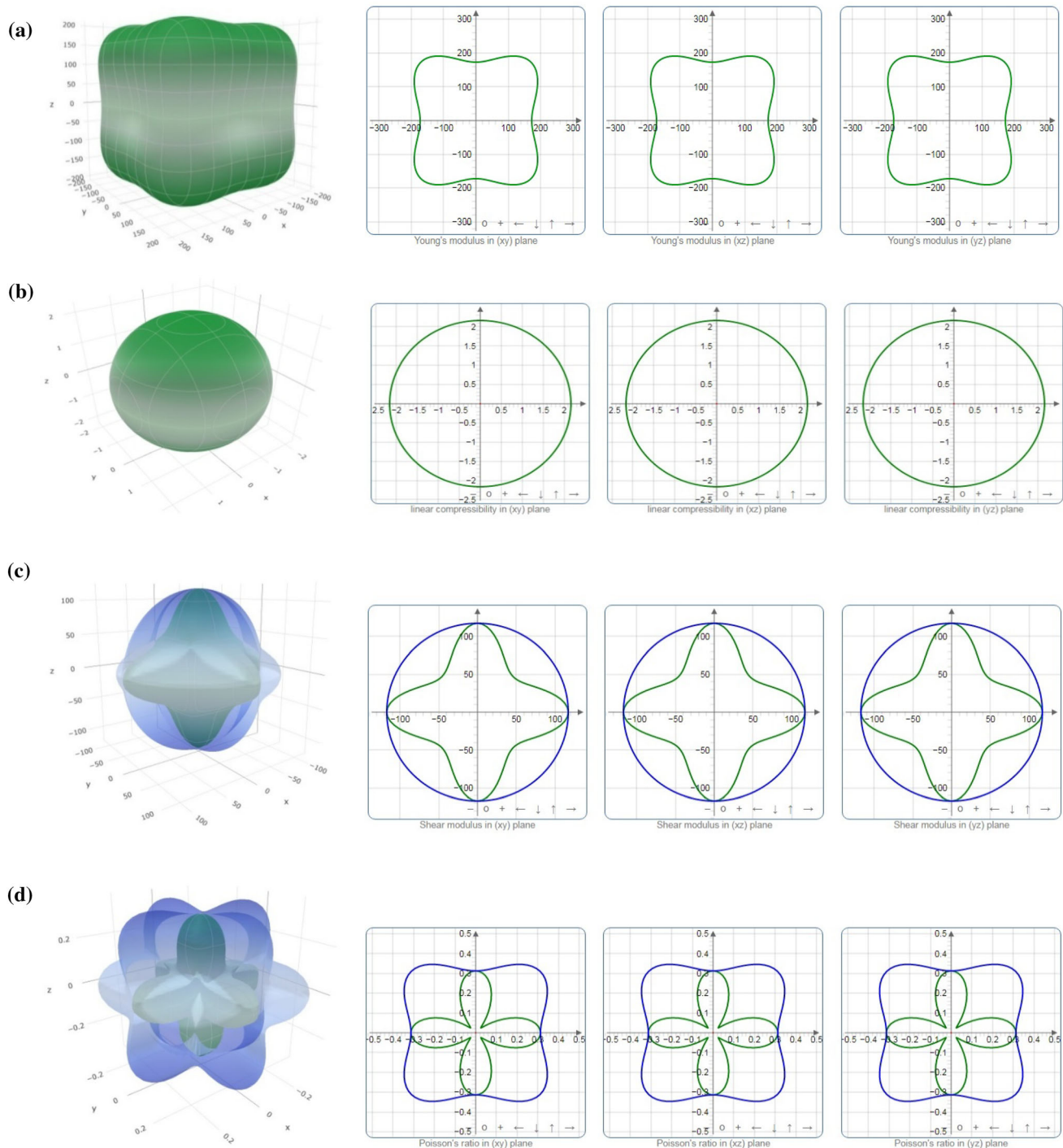


Figure 2. Spatial dependence of (a) Young’s modulus, (b) linear compressibility, (c) shear modulus and (d) Poisson’s ratio of LiNbCoAl in 3D and 2D (xy, xz and yz planes).

property for each of the materials tested, but Young’s modulus, Shear modulus and Poisson ratio are determined to be anisotropic qualities. The deviation from spherical symmetry is evident from the calculated anisotropic factor listed in table 3. Another strain-related metric is the Kleinman (ξ) parameter, which may be computed as

$\xi = \frac{C_{11}+8C_{12}}{7C_{11}-2C_{12}}$ [63]. A low value of ξ near 0 indicates resistance for the bond-angle distortion, while a high value of near 1 indicates minimum bond stretching. The anticipated values for LiNbCoAl and LiNbCoGa in this situation are 0.76 and 0.80, respectively, demonstrating that bending will prevail out in both materials under stress.

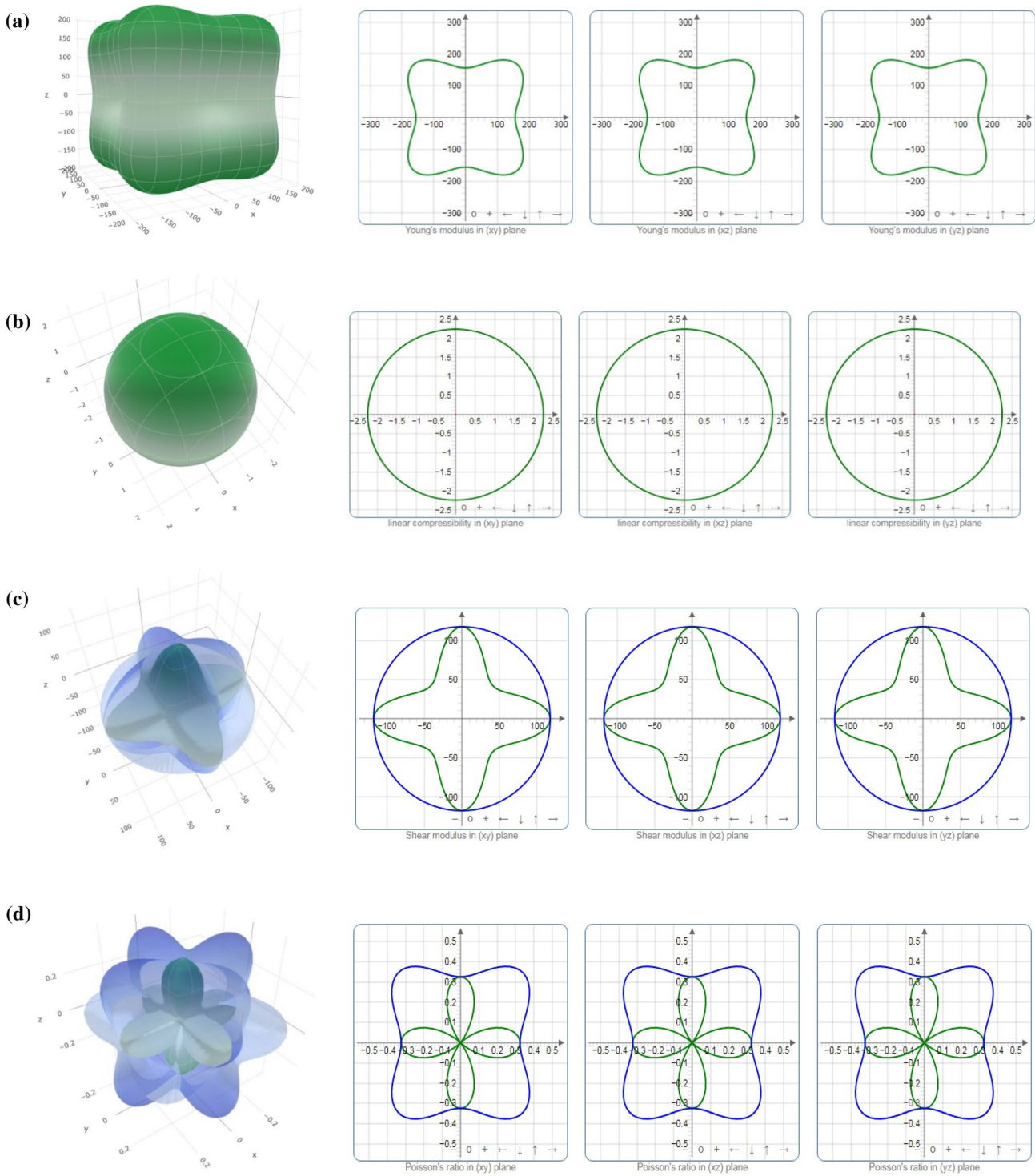


Figure 3. Spatial dependence of (a) Young's modulus, (b) linear compressibility, (c) shear modulus and (d) Poisson's ratio of LiNbCoGa in 3D and 2D (xy, xz and yz planes).

3.3 Thermodynamic properties

The primary parameter for analysing the thermodynamics is Debye's temperature (θ_D), which is dependent on the elastic constants, specific heat and melting point. It is determined

using compressional sound velocities, average sound velocities and shear velocities (v_s , v_m and v_l).

$$\theta_D = \frac{\hbar}{k_B} \left(\frac{3n\rho N_A}{4\pi M} \right)^{1/3} \left(\frac{1}{3} \left[\frac{1}{v_l^3} + \frac{1}{v_t^3} \right] \right)^{-1/3} \quad (9)$$

Table 3. Calculated anisotropic factors of the presented QH compounds.

Mechanical parameters	Range	LiNbCoAl	LiNbCoGa
Young's modulus	E_{\min}	172.6	156.12
	E_{\max}	280.41	279.12
Linear compressibility (β in TPa^{-1})	β_{\min}	2.1635	2.2431
	β_{\max}	2.1635	2.2431
Shear modulus (GPa)	G_{\min}	65.714	58.917
	G_{\max}	117.16	117.58
Poisson's ratio	ν_{\min}	0.035054	-0.0083763
	ν_{\max}	0.44022	0.4853

The symbols here have their conventional meanings. In terms of compressional velocity (v_l) and shear velocity (v_s), the average sound velocity (v_m) can be expressed as [64,65]:

$$v_m = \left(\frac{1}{3} \left[\frac{1}{v_l^3} + \frac{1}{v_s^3} \right] \right)^{-1/3} \quad (10)$$

The material's density and shear modulus (G) both affect the shear velocity.

$$v_s = \sqrt{\frac{G}{\rho}} \quad (11)$$

Similar to the bulk and shear moduli, the density of the material and the compressional velocity are correlated.

$$v_l = \sqrt{\frac{3B + 4G}{3\rho}} \quad (12)$$

From the relationships existing between the compressional velocity and shear velocity, the average sound velocity (v_m) is calculated as:

$$v_m = \left(\frac{1}{3} \right)^{1/3} \left(\frac{2}{v_s^2} + \frac{1}{v_l^3} \right)^{-1/3} \quad (13)$$

The melting values (points) of both alloys, calculated here using equation (5), are also shown in table 4 to be of paramount importance in the presented research work. Table 4 also includes very significant comparisons of the

computed Debye's temperature and the three material velocities to those of other compounds of the same category. Table 4 shows that, with the exception of CoZrMnGe of the same type, both QHs have a greater Debye's temperature than the two materials analysed. As a result, the lattice thermal conductivity can also be high. In a similar vein, considering a material's thermal response is crucial because it has a big impact on how it performs in electrical and electronic applications.

The material's lattice vibrations have a direct impact on the thermal response. In order to understand the thermal vibrations shown in figure 4, the behaviour of the material's specific heat at constant volume (C_V), entropy (S), and vibrational free energy (F) can be used to analyse its thermal response. The equation [66] can be used to determine the specific heat at constant volume (C_V) at various temperatures (between 100 and 1600 K):

$$C_V = k_B \int_0^\infty \frac{\left(\frac{\hbar\omega}{k_B T} \right)^2 \exp\left(\frac{\hbar\omega}{k_B T} \right)}{\left(\exp\left(\frac{\hbar\omega}{k_B T} \right) - 1 \right)^2} D(\omega) d\omega \quad (14)$$

where $D(\omega)$ is the phonon density of states and k_B the Boltzmann constant. This is supported by the observation that C_V expands quickly as the temperature rises up to 200 K. Dulong-law and Petit's law ($C_V = 3nR$), where n is the number of atoms per unit cell and R the universal gas constant explain its behaviour at 200 K, which is consistent with Debye's model ($C_V \propto T^3$). According to this law, after 200 K the C_V attains a constant value of

Table 4. Calculated velocities (m/s) and the other material parameters.

QH compound	v_s	v_l	v_m	θ_D	$T_{\text{melt}} \pm 300 \text{ K}$	Ref.
LiNbCoAl	3577	6188	4607	495	1996	This study
LiNbCoGa	3192	5530	4122	443	1912	
CoZrMnGa	2911.98	5378.52	3249.61	401.92	1823.10	[15]
CoZrMnGe	2292.71	5420.32	3638.60	449.57	1961.85	[15]
CoZrMnIn	2820.77	5303.74	3151.85	374.50	1792.02	[15]

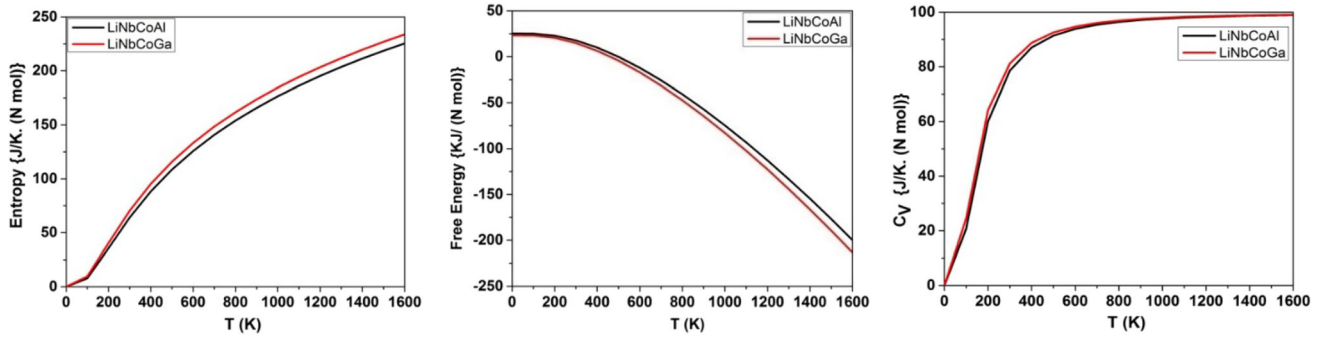


Figure 4. Response of the thermodynamic properties for both the investigating materials.

$98.768 \text{ J K}^{-1} \text{ mol}^{-1}$. There are also the vibrational frequencies that lead to the vibrational free energy (F). Similarly, as the temperature increase this vibrational free energy (F) decreases, which can be explained by the following relation of entropy (S) and enthalpy (E):

$$F = E - TS \quad (15)$$

The crystal's lattice vibrations at absolute zero temperature are depicted by a significant value of F at 0 K. Entropy (S), a measure of disorder, however, increases as temperature rises. In turn, as can be shown in figure 4, the vibrational free energy (F) decreased with increasing temperature.

3.4 Thermoelectric properties

A conflict exists among the several thermoelectric factors that influence a material's thermoelectric performance to analyse all the thermoelectric characteristics over the entire temperature range of 300 to 1600 K, including the Seebeck coefficient, electrical conductivity, electronic thermal conductivity and figure of merit, due to the high melting temperatures of the recommended QH alloys. Even the thermoelectric properties signifies, by the band structure of the presenting alloys and analyse their potential as thermoelectrics in extremely hot environments. Here, the constant relaxation time is used to describe all thermoelectric properties, i.e., $\tau = 10^{-14} \text{ s}$.

3.4a Band structure of the presenting alloys: The band structure of both the presenting QH alloys are presented in figure 5 for the better understanding of electrical properties as well as for the thermoelectric performance of the materials. It can be observed that for both the alloys the valence band maxima and the conduction band minima are lying at the W and X points of the Brillouin zone, respectively, and hence there is the indirect bandgap. Along with the band structure the total density of states and the partial density of states are also plotted to get an idea about the atomic contributions. It can also be depicted that in both the QH alloys the d-orbitals of

Nb (Niobium) have major contribution in the valence bands as well as in the conduction bands of both the alloys. There is also the presence of triply degenerate state in the valence band near the Fermi level, which will affect (increase) the Seebeck coefficient values of both the presenting alloys, which can be explained by the Mott relation given below:

$$S = \frac{4\pi^2 k_B^2}{eh^2} \left(\frac{4\pi}{3n} \right)^{2/3} m^* T \quad (16)$$

where k_B is the Boltzmann constant, h the Planck's constant, n stands for the carrier concentration, m^* for the effective mass of the charge carrier and T the absolute temperature. The above equation shows the direct impact of effective mass (m^*) on the Seebeck coefficient (S) and the effective mass also depends on the band degeneracy as:

$$m^* = N_v^{2/3} m_b^* \quad (17)$$

here, m_b^* and N_v are the effective mass corresponding to a single valley degeneracy, which can increase, and the band degeneracy. Hence it can implicit that due to the triply degenerate state there will be increase in the effective mass and hence the Seebeck coefficient [67]. As there is a significant impact of Seebeck coefficient on the figure of merit (ZT); it also enhanced the considerable limits..

3.4b Seebeck coefficient: The Seebeck coefficient, which gauges how much thermoelectric voltage a material produces while maintaining a temperature gradient, is the main thermoelectric parameter. For both of the presented QH compounds, complete behaviour can be analysed from figure 6, in which it is presented at the five different temperatures with the chemical potential μ (eV). The positive range of chemical potential (μ) indicates the n-type doping of the material, whereas the negative range indicates the p-type doping. The values of the Seebeck coefficient for both compounds, shown in figure 6, decrease with increasing temperature. At 300 K, the maximum Seebeck coefficients for LiNbCoAl and LiNbCoGa are 1307 and $1575 \mu\text{V K}^{-1}$, respectively. However, for both materials, it got decreasing with an increase in temperature.

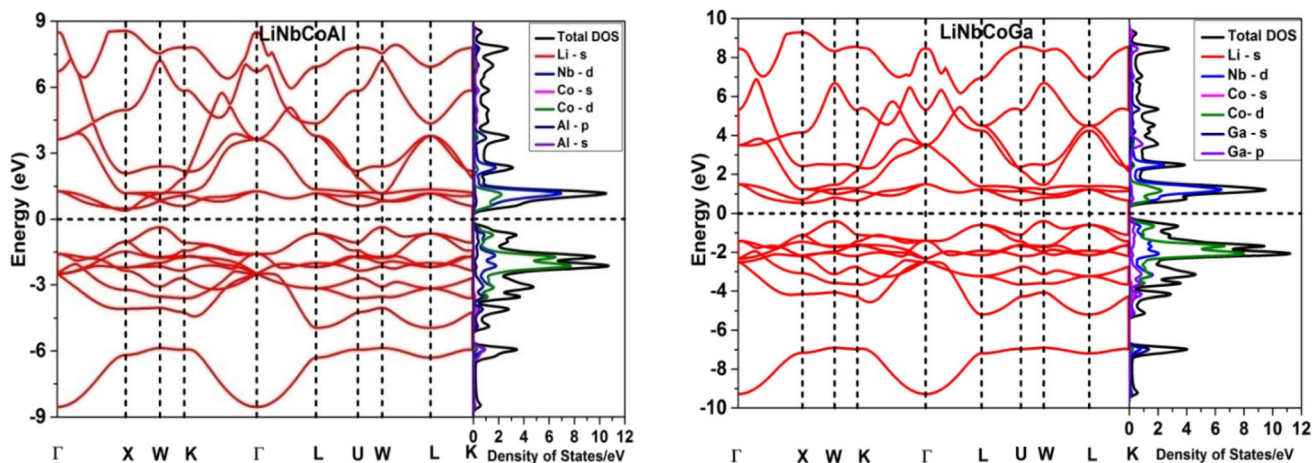


Figure 5. Description of band structure of the presenting quaternary Heusler alloys.

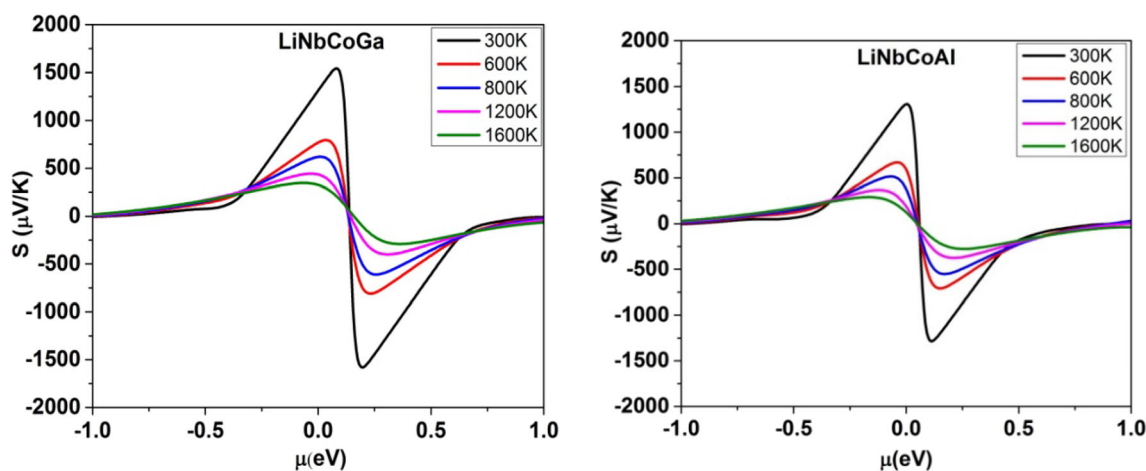


Figure 6. Variation of Seebeck coefficient for both the QHs.

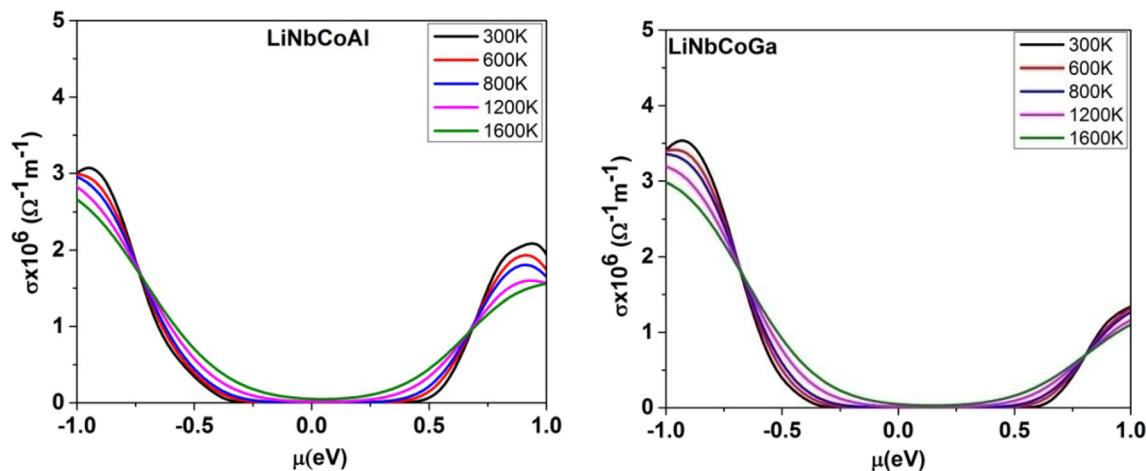


Figure 7. Variations of electrical conductivity of both the presenting QHs.

3.4c *Electrical conductivity:* The plot of figure 7 shows the electrical conductivities of both materials with chemical potentials (in the range of -1.0 to $+1.0$ eV). At 0.0 eV of

the chemical potential, it is found that the electrical conductivity of LiNbCoAl is zero, and it then increases on both sides. Then it got increasing with an increase in

temperature and the curves overlaps at 0.69 and 0.73 eV for the n-type and p-type doping regions and then the electrical conductivity showed the inverse behaviour with temperature. The maximum value recorded is $3.07 \times 10^6 \Omega^{-1} \text{m}^{-1}$ for the p-type doping. Similar behaviour for LiNbCoGa can be observed with maximum electrical conductivity of $3.53 \times 10^6 \Omega^{-1} \text{m}^{-1}$ for the p-type doping. Hence, the electrical conductivities of both the presenting QH alloys indicate their p-type semiconducting nature, and the entire behaviour can be viewed in figure 7.

The electrical conductivity (σ) values for both the compounds are showing the inverse behaviour (decreasing with increase in temperature) due to the mobility (μ), as we know that $\sigma = ne\mu$. In same quest we also have to take into account that due to the intrinsic scattering the mobility depends upon the temperature ($\mu \propto T^{-1/3}$). Hence as the temperature will increase the mobility will decrease and it affects the electrical conductivity, which is why the electrical conductivity (σ) shows the inverse behaviour in this research work.

3.4d Electronic and lattice thermal conductivity: In both QH alloys, when the temperature increases, the electronic thermal conductivity (k_e), which quantifies the free-electron vibrations in a material, also increases. Electronic thermal conductivity peaks for LiNbCoAl and LiNbCoGa occur at $71.2 \text{ Wm}^{-1} \text{K}^{-1}$ (n-type doping) and $71.5 \text{ Wm}^{-1} \text{K}^{-1}$ (p-type doping) at 1600 K, respectively. However, these changes can be examined from figure 8.

Similar to this, the widely used Slack equation [68] provides a method for determining the vibrational response of a lattice as a function of temperature (the lattice thermal conductivity).

$$k_l = \frac{AM\theta_D^3 V^{1/3}}{\gamma^2 T n^{2/3}} \quad (18)$$

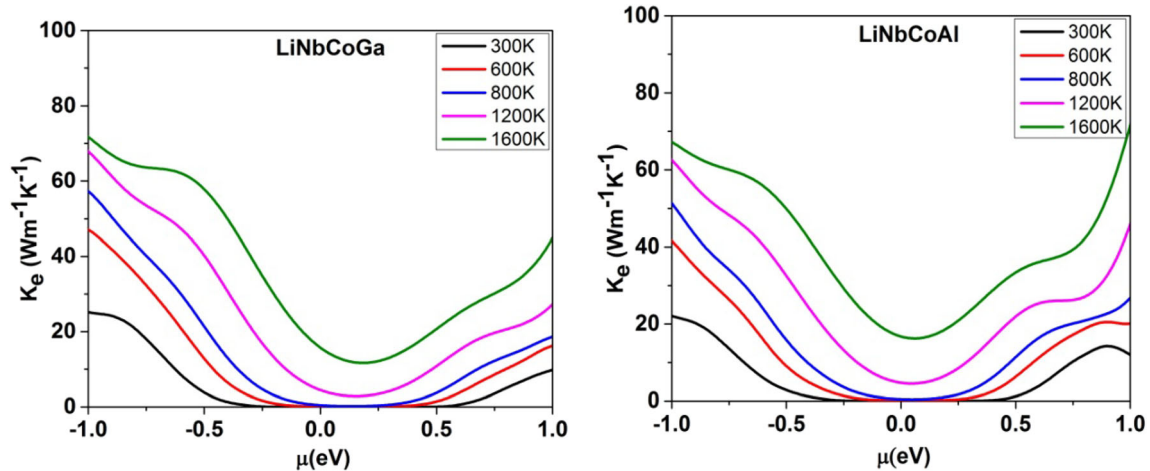


Figure 8. Electronic thermal conductivities of LiNbCoAl and LiNbCoGa with respect to chemical potential.

The symbols used here have their usual meanings. Similarly, the coefficient ‘A’ depending upon γ [69,70] is expressed as:

$$A(\gamma) = \frac{5.720 \times 0.849 \times 10^7}{\left[1 - \left(\frac{0.514}{\gamma}\right) + \left(\frac{0.228}{\gamma^2}\right)\right]} \quad (19)$$

The Gruneisen parameter can be calculated by using Poisson’s ratio (ν) with the following equation:

$$\gamma = \frac{3(1 + \nu)}{2(2 - 3\nu)} \quad (20)$$

A presentation of the predicted lattice thermal conductivity and the Gruenisen parameter for each of the alloys is shown in figure 9. Increasing phonon scattering causes the lattice thermal conductivity to decrease at a rate proportional to temperature ($1/T$). To explain this behaviour, phonon group velocity and Gruenisen parameter are analysed using py script. The phonon group velocity is found to be 4524 and 4065 m s^{-1} for LiNbCoAl and LiNbCoGa, respectively, which are very close to the values obtained using thermal pw.x package. With respect to change in volume, the change in phonon frequency is investigated to calculate the value of Gruenisen parameter, which turns out to be 0.320 and 0.551 for LiNbCoAl and LiNbCoGa, respectively, at room temperature. The Gruenisen parameter is a measure of anharmonicity and thus scattering of phonons in the crystal. The lower value of phonon group velocity and higher value of Gruenisen parameter of LiNbCoGa verify its lower value of lattice thermal conductivity compared to LiNbCoAl. In accordance with the thermoelectric properties, the lattice thermal conductivity was examined in the 300 to 1600 K temperature range. Therefore, it is simple to see how total thermal conductivity ($k_t = k_e + k_l$) affects the figure of merit.

3.4e Figure of Merit (ZT): One of the most fascinating metrics for describing a material’s thermoelectric activity is

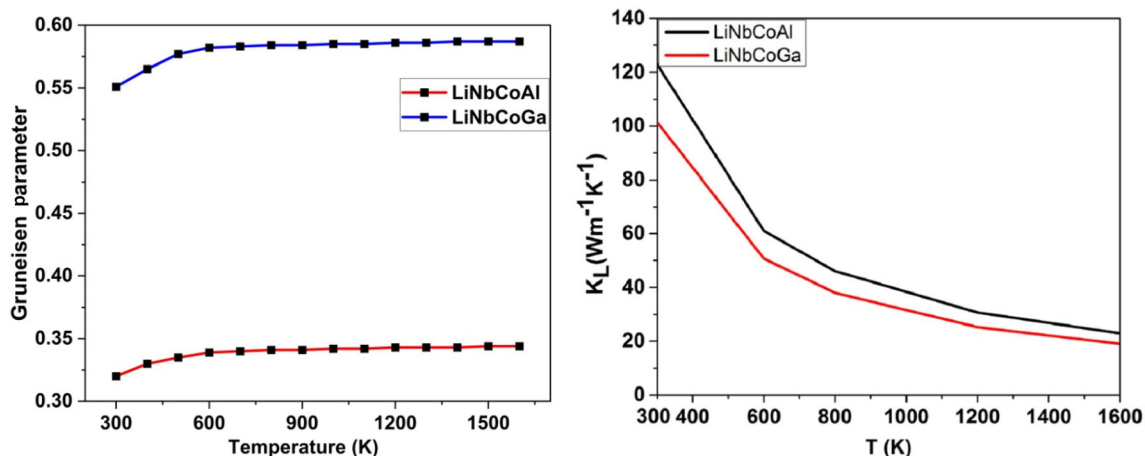


Figure 9. Gruneisen parameter and the temperature-dependent lattice thermal conductivity.

the Figure of Merit. Due to its reliance on the fundamental thermoelectric property known as the Seebeck coefficient as well as the contradicting nature of electrical and thermal conductivities, it also becomes quite fascinating. Its dimensionless relationship is as follows:

$$ZT = \frac{S^2\sigma}{k_e + k_l} T \tag{21}$$

The figure of merit (ZT) is described for both of the QH alloys across a wide temperature range (300 to 1600 K) based on the other thermoelectric properties. It may be seen in figure 10, its effectiveness is illustrated by the linear relationship between ZT and temperature. ZT values of 0.47 for LiNbCoAl and 0.56 for LiNbCoGa have been measured for p-type doped regions at 1600 K. It claims that the QHs that are being shown are useful as high-temperature thermoelectric components.

In order to assess the validity of the current work, Table 5 compares the figures of merit of these compounds to those of newly found or researched Li-based

Table 5. Comparing the highest ZT to other QH compounds.

Material	T (K)	ZT	Ref.
LiNbCoAl	1600	0.47	This study
LiNbCoGa	1600	0.56	
LiScPdPb	1200	0.19	[37]
LiTiCoSn	1600	0.43	[71]
LiYNiSn	700	0.14	[72]
LiTiCoGe	700	0.14	[38]
LiTiCoSi	700	0.10	[38]

non-magnetic QH compounds. The same approximations for the constant relaxation time, or for $\tau = 10^{-14}$ s, are used to examine all of the materials being compared. However, it is evident from the comparison that the investigated QH materials have better thermoelectric performance.

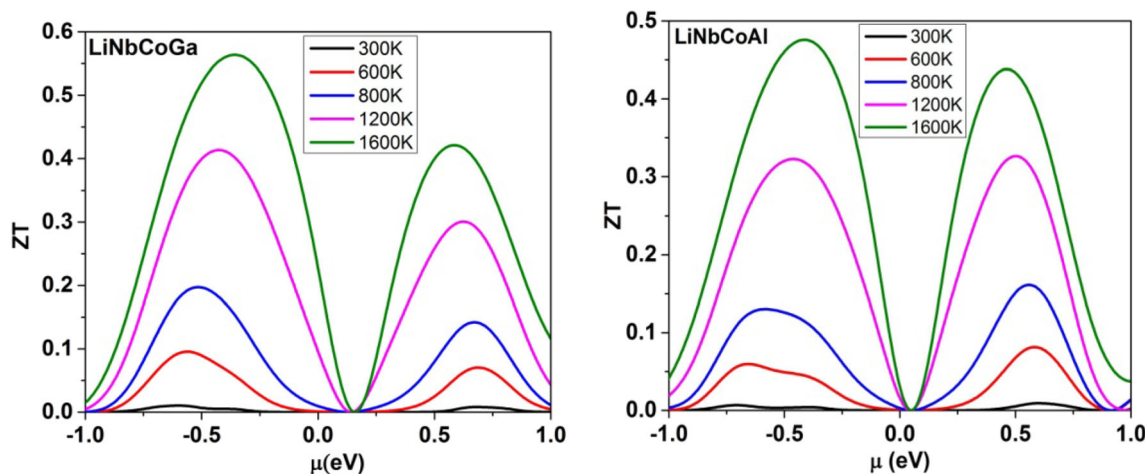


Figure 10. Variations of Figure of Merit (ZT) of both the compounds with the chemical potential.

4. Conclusions

The theoretical research approach of DFT evaluated the various properties of the presented compounds in the high-temperature range of 1600 K as per their high melting points, i.e., (1996 ± 300 K for LiNbCoAl) and (1912 ± 300 K for LiNbCoGa). For both the compounds, phonon dispersion curves (vibrational characteristics) have shown along the K-points of the Brillouin zone to assure dynamical stability. To seek practical reliability, all the mechanical and elastic properties are calculated, whereas the bulk modulus and hardness for LiNbCoAl and LiNbCoGa are recorded as 154 GPa, 148 GPa and 12.19, 12.20, respectively. The indirect bandgap and the semiconducting nature for both the presenting alloys has been discussed along with its significance in thermoelectric performances. In the quest for their high melting points, all the thermodynamic parameters as well as the thermoelectric properties are explored and discussed in the temperature range of 1600 K. The peak figure of merit (ZT) of 0.47 and 0.56 for the studied materials of LiNbCoAl and LiNbCoGa, respectively, has been attained at 1600 K. The dimensional dependence and the isotropic nature of all the mechanical properties are analysed under the aegis of the ELATE online package. This leads to the conclusion that linear compressibility is an isotropic property for each of the materials under consideration, while Young's modulus, Shear modulus, and Poisson ratio are anisotropic quantities. However, the figure of merit appears to be of average performance but it is better than many of the other reported compounds of the same kind, even it can be improved by the pressure techniques and doping methods. Finally, this study is an outlet for theoretical research which can lead to a few of the important foundations and implementations in experimental research of energy conversions.

References

- [1] Sztékler K, Wojciechowski K and Komorowski M 2017 *E3S Web Conf.* **14** 01032
- [2] Ghoshal U and Guha A 2009 *J. Electron. Mater.* **38** 1148
- [3] Strasser M, Aigner R, Lauterbach C, Sturm T F, Franosch M and Wachutka G 2004 *Sens. Actuators A Phys.* **114** 362
- [4] Choi H S, Yun S and Whang K 2007 *Appl. Therm. Eng.* **27** 2841
- [5] Champier D 2017 *Energy Convers. Manag.* **140** 167
- [6] Ismail B and Ahmed W 2009 *Recent Patents Electr. Eng.* **2** 27
- [7] Kaur K, Kumar R and Rai D P 2018 *J. Alloys Compd.* **763** 1018
- [8] Yamashita O, Tomiyoshi S and Makita K 2003 *J. Appl. Phys.* **93** 368
- [9] Tang Y, Gibbs Z M, Agapito L A, Li G, Kim H S, Nardelli M B *et al* 2015 *Nat. Mater.* **14** 1223
- [10] Caillat T, Borshchevsky A and Fleurial J P 1996 *J. Appl. Phys.* **80** 4442
- [11] Khandy S A, Islam I, Gupta D C, Khenata R and Laref A 2019 *Sci. Rep.* **9** 1475
- [12] Kaur K and Kaur J 2017 *J. Alloys Compd.* **715** 297
- [13] Kaur K 2017 *Europhys. Lett.* **117** 47002
- [14] Inomata K, Ikeda N, Tezuka N, Goto R, Sugimoto S, Wojcik M *et al* 2008 *Sci. Technol. Adv. Mater.* **9** 014101
- [15] Hossain M A, Rahman M T, Khatun M and Haque E 2018 *Comput. Condens. Matter* **15** 31
- [16] Casper F, Graf T, Chadov S, Balke B and Felser C 2012 *Semicond. Sci. Technol.* **27** 063001
- [17] Kieven D, Klenk R, Naghavi S, Felser C and Gruhn T 2010 *Phys. Rev. B* **81** 075208
- [18] Slack G A and Rowe D M 1995 *CRC Handbook of thermoelectrics* (Boca Raton: CRC Press) p 407
- [19] Misra D K, Bhardwaj A and Singh S 2014 *J. Mater. Chem. A* **2** 11913
- [20] Xie W, Weidenkaff A, Tang X, Zhang Q, Poon J and Tritt T M 2012 *Nanomaterials* **2** 379
- [21] Young D P, Khalifah P, Cava R J and Ramirez A P 2000 *J. Appl. Phys.* **87** 317
- [22] Culp S R, Simonson J W, Poon S J, Ponnambalam V, Edwards J and Tritt T M 2008 *Appl. Phys. Lett.* **93** 022105
- [23] Jong J Y, Zhu J, Jon M G, Zhou Y, Kim J and Yan J 2017 *J. Alloys Compd.* **693** 462
- [24] Fang T, Zheng S, Zhou T, Yan L and Zhang P 2017 *Phys. Chem. Chem. Phys.* **19** 4411
- [25] Yu C, Zhu T J, Shi R Z, Zhang Y, Zhao X B and He J 2009 *Acta Mater.* **57** 2757
- [26] Sakurada S and Shutoh N 2005 *Appl. Phys. Lett.* **86** 082105
- [27] Berry T, Fu C, Auffermann G, Fecher G H, Schnelle W, Serrano-Sanchez F *et al* 2017 *Chem. Mater.* **29** 7042
- [28] Chen S and Ren Z 2013 *Mater. Today* **16** 387
- [29] Poon S J, Wu D, Zhu S, Xie W, Tritt T M, Thomas P *et al* 2011 *J. Mater. Res.* **26** 2795
- [30] Fu C, Bai S, Liu Y, Tang Y, Chen L, Zhao X *et al* 2015 *Nat. Commun.* **6** 8144
- [31] Fu C, Wu H, Liu Y, He J, Zhao X and Zhu T 2016 *Adv. Sci.* **3** 1600035
- [32] Yu J, Fu C, Liu Y, Xia K, Aydemir U, Chasapis T C *et al* 2018 *Adv. Energy Mater.* **8** 1701313
- [33] Xue Q Y, Liu H J, Fan D D, Cheng L, Zhao B Y and Shi J 2016 *Phys. Chem. Chem. Phys.* **18** 17912
- [34] He J, Amsler M, Xia Y, Naghavi S S, Hegde V I, Hao S *et al* 2016 *Phys. Rev. Lett.* **117** 046602
- [35] Haleoot R and Hamad B 2020 *J. Phys. Condens. Matter* **32** 075402
- [36] Kara H, Kahaly M U and Özdoğan K 2018 *J. Alloys Compd.* **735** 950
- [37] Gupta Y, Sinha M M and Verma S S 2021 *J. Solid State Chem.* **304** 122601
- [38] Singh J, Kaur K, Khandy S A, Dhiman S, Goyal M and Verma S S 2021 *Int. J. Energy Res.* **45** 16891
- [39] He J, Naghavi S S, Hegde V I, Amsler M and Wolverton C 2018 *Chem. Mater.* **30** 4978
- [40] Rafique M, Uqaili M A, Shuai Y, Mahar M A and Ahmed I 2018 *Appl. Surf. Sci.* **458** 145
- [41] Rafique M, Uqaili M A, Mirjat N H, Tunio M A and Shuai Y 2019 *Phys. E Low-dimens. Syst. Nanostruct.* **109** 169

- [42] Khandy S A, Islam I, Gupta D C, Bhat M A, Ahmad S, Dar T A *et al* 2018 *RSC Adv.* **8** 40996
- [43] Perdeu J P, Burke K and Ernzerhof M 1996 *Phys. Rev. Lett.* **77** 3865
- [44] Giannozzi P, Baroni S, Bonini N, Calandra M, Car R, Cavazzoni C *et al* 2009 *J. Phys. Condens. Matter* **21** 395502
- [45] Monkhorst H J and Pack J D 1976 *Phys. Rev. B* **13** 5188
- [46] Barreteau C, Pan L, Amzallag E, Zhao L D, Bérardan D and Dragoe N 2014 *Semicond. Sci. Technol.* **29** 064001
- [47] Dal Corso A 2016 *J. Phys. Condens. Matter* **28** 075401
- [48] Gaillac R, Pullumbi P and Coudert F X 2016 *J. Phys. Condens. Matter* **28** 275201
- [49] Baroni S, Giannozzi P and Testa A 1987 *Phys. Rev. Lett.* **58** 1861
- [50] Scheidemantel T J, Ambrosch-Draxl C, Thonhauser T, Badding J V and Sofo J O 2003 *Phys. Rev. B* **68** 125210
- [51] Jodin L, Tobola J, Pecheur P, Scherrer H and Kaprzyk S 2004 *Phys. Rev. B* **70** 184207
- [52] Madsen G K and Singh D J 2006 *Comput. Phys. Commun.* **175** 67
- [53] Goyal M and Sinha M M 2021 *J. Phys. Chem. Solids* **153** 110024
- [54] Ryu B and Oh M W 2016 *J. Korean Ceram. Soc.* **53** 273
- [55] Mohamedi M W, Chahed A, Amar A, Rozale H, Lakdja A, Benhelal O *et al* 2016 *Eur. Phys. J. B* **89** 267
- [56] Fine M E, Brown L D and Marcus H L 1984 *Scr. Metall.* **18** 951
- [57] Sinha M M and Sharma A 2009 *Phys. B Condens. Matter.* **404** 1187
- [58] Pugh S F 1954 *London, Edinburgh Dublin Philos. Mag. J. Sci.* **45** 823
- [59] Born M and Huang K 1954 *Dynamical theory of crystal lattices* (Oxford: Clarendon Press)
- [60] Voigt W 1928 *Text book of crystal physics* (Leipzig Berlin: G.B. Teubner)
- [61] Hill R 1952 *Proc. Phys. Soc. Sect. A* **65** 349
- [62] Chen X Q, Niu H, Li D and Li Y 2011 *Intermetallics* **19** 1275
- [63] W A Harrison 1989 (Dover: New York), p 176
- [64] Kleinman L 1962 *Phys. Rev.* **128** 2614
- [65] Schreiber E, Anderson O L, Soga N and Bell J F 1974 *Elastic constants and their measurement* (New York: McGraw-Hill)
- [66] Tani J I and Kido H 2008 *Comput. Mater. Sci.* **42** 531
- [67] Singh J, Kaur K, Bhatt M A, Sharopov U B, Dhiman S, Goyal M *et al* 2022 *Mater. Today Commun.* **32** 103961
- [68] Morelli D T and Slack G A 2006 *High thermal conductivity materials* (New York: Springer-Verlag)
- [69] Belomestnykh V N and Tesleva E P 2004 *Tech. Phys.* **49** 1098
- [70] Julian C L 1965 *Phys. Rev.* **137** A128
- [71] Singh J, Kaur K, Khandy S A, Goyal M, Dhiman S and Verma S S 2022 *Mater. Today Proc.* **57** 211
- [72] Singh J, Kaur K, Goyal M, Khandy S A, Dhiman S and Verma S S 2021 *AIP Conf. Proc.* **2352** 020028